January 2011

Loading mechanics of the femur in tiger salamanders (Ambystoma tigrinum) during terrestrial locomotion

K. Megan Sheffield
University of South Florida, msheff@clemson.edu

Richard W. Blob
Clemson University

The Journal of Experimental Biology 214, 2603-2615

doi:10.1242/jeb.048736

RESEARCH ARTICLE

Loading mechanics of the femur in tiger salamanders (*Ambystoma tigrinum*) during terrestrial locomotion

K. Megan Sheffield* and Richard W. Blob†

Department of Biological Sciences, Clemson University, Clemson, SC 29634 USA

*Present address: Department of Academic Services, University of South Florida, Tampa, FL 33620 USA
†Author for correspondence (rblob@clemson.edu)

Accepted 9 May 2011

SUMMARY

Salamanders are often used as representatives of the basal tetrapod body plan in functional studies, but little is known about the loads experienced by their limb bones during locomotion. Although salamanders' slow walking speeds might lead to low locomotor forces and limb bone stresses similar to those of non-avian reptiles, their highly sprawled posture combined with relatively small limb bones could produce elevated limb bone stresses closer to those of avian and mammalian species. This study evaluates the loads on the femur of the tiger salamander (*Ambystoma tigrinum*) during terrestrial locomotion using three-dimensional measurements of the ground reaction force (GRF) and hindlimb kinematics, as well as anatomical measurements of the femur and hindlimb muscles. At peak stress (29.8±2.0% stance), the net GRF magnitude averaged 0.42 body weights and was directed nearly vertically for the middle 20–40% of the contact interval, essentially perpendicular to the femur. Although torsional shear stresses were significant (4.1±0.3 MPa), bending stresses experienced by the femur were low compared with other vertebrate lineages (tensile: 14.9±0.8 MPa; compressive: –18.9±1.0 MPa), and mechanical property tests indicated yield strengths that were fairly standard for tetrapods (157.1±3.7 MPa). Femoral bending safety factors (10.5) were considerably higher than values typical for birds and mammals, and closer to the elevated values calculated for reptilian species. These results suggest that high limb bone safety factors may have an ancient evolutionary history, though the underlying cause of high safety factors (e.g. low limb bone loads, high bone strength or a combination of the two) may vary among lineages.

Key words: locomotion, biomechanics, force, bone, stress, safety factor, salamander.

INTRODUCTION

The limb bones of tetrapods exhibit a wide range of shapes and sizes. Because locomotion is one of the most frequent and demanding behaviors in which limbs are used (Biewener, 1990; Biewener, 1993), this diversity in limb design is frequently attributed to variation in the mechanical loads that bones experience during locomotion (Currey, 1984; Bertram and Biewener, 1988; Blob, 2001; Currey, 2002; Lieberman et al., 2004; de Margerie et al., 2005). Damage or fracture of bones during locomotion could have serious, even fatal, consequences for animals. However, limb bones can usually withstand loads much higher than they normally experience before they fail, a margin of protection known as a safety factor (Alexander, 1981; Biewener, 1993; Blob and Biewener, 1999). High safety factors provide insurance against failure, but could also make limb bones more costly to grow, maintain and transport (Diamond, 1998).

The ability of a limb bone to withstand loads depends on the magnitude of the load, the loading regime in which it is applied and the mechanical properties of the bone. Several studies have examined the relationships between these factors in birds and mammals (e.g. Rubin and Lanyon, 1982; Biewener, 1983a; Biewener, 1983b; Biewener et al., 1983; Biewener et al., 1988; Carrano, 1998; Demes et al., 2001; Lieberman et al., 2004; Main and Biewener, 2004; Main and Biewener, 2007), lineages in which the limbs move primarily in a parasagittal plane during locomotion. With this pattern of movement, limb bones of quadrupedal mammals are loaded mainly in bending and axial compression, with torsion also prominent in the hindlimbs of bipedal birds (Carrano, 1998; Main and Biewener, 2007). Birds and mammals also typically have limb bone safety factors between two and four (Alexander, 1981; Biewener, 1993), with generally similar limb bone mechanical properties (Biewener, 1982; Erickson et al., 2002). However, studies of reptilian species that use a sprawling limb posture have shown loading patterns that differ substantially from those of birds and mammals. For example, studies in lizards and crocodilians (Blob and Biewener, 1999; Blob and Biewener, 2001), as well as turtles (Butcher and Blob, 2008), have found much greater limb bone torsion than in quadrupedal mammals, but also higher safety factors (more than 10 in bending and five in shear) that were related to both lower locomotor loads and greater resistance to failure. One possible explanation for the differences in safety factors found between non-avian reptiles and other amniote lineages is that high limb bone safety factors are adaptations that help accommodate a variety of demands in reptiles, including high variability in load magnitudes and low rates of bone remodeling and repair (Blob and Biewener, 1999; Blob and Biewener, 2001) (but see Ross and Metzger, 2004). It is also possible that, based on the lineages from which data are available, the loading patterns of non-avian reptiles are retained ancestral conditions. Such loading patterns thus might, or might not, be adaptive for non-avian reptiles, but, as ancestral retentions, would indicate that birds and mammals had diverged independently with regard to these traits (Blob and Biewener, 1999; Blob and Biewener, 2001; Butcher and Blob, 2008).

To clarify whether the bone loading patterns observed in non-avian reptiles are ancestral or derived conditions, data from species

outside the amniote clade would provide crucial perspective. Salamanders are an ideal group from which such data can be obtained. As amphibians, they are members of the clade that is the outgroup to the amniotes (Carroll and Holmes, 1980; Gao and Shubin, 2001). In particular, they are the only group of living amphibians with locomotor habits comparable to most other tetrapods in which bone loading has been evaluated, because caecilians are limbless and frogs are specialized for saltatory locomotion (Liem et al., 2001). As a result of their phylogenetic position and unspecialized body plan, salamanders are often used as a model for the first terrestrial vertebrates in locomotor studies (Ashley et al., 1991; Ashley-Ross, 1994a; Ashley-Ross, 1994b; Ashley-Ross, 1995; Ashley-Ross and Lauder, 1997; Ashley-Ross and Barker, 2002; Ashley-Ross and Bechtel, 2004; Reilly et al., 2006). But in addition to the phylogenetic significance of salamanders, aspects of their morphology and locomotor habits also generate questions about how their limbs might be loaded. For example, salamanders have three or four legs on the ground for 59.4% of their stride (Ashley-Ross, 1994a) and have a fairly sedentary lifestyle, leading to expectations of low limb bone loads and high safety factors. However, salamanders also have relatively small limb bones for their size. Based on published regression equations (Blob, 2000), lizards with a body mass similar to mature tiger salamanders (80 g) would have a mean femur diameter of 2.02 mm. Our anatomical data (Table 1) indicate salamanders of this size have femora that are only 1.88 mm in mean diameter, nearly 10% narrower than similarly sized lizards. With sprawling posture and a long tail dragging during locomotion (Reilly et al., 2005), high stresses (particularly torsional) might be placed on bones that are not very robust, leading to a low safety factor.

To test these ideas, we used three-dimensional force platform and kinematic data, combined with a musculoskeletal model, to evaluate femoral stresses during terrestrial walking in tiger salamanders, *Ambystoma tigrinum* Green 1825. We then compared these stresses with bone mechanical property data to calculate femoral safety factors. Although salamander limbs are too small to allow implantation of strain gauges to directly measure bone deformations (Biewener, 1992), force platform studies can provide insights into the orientation and magnitude of forces and moments acting on limb bones (Biewener and Full, 1992), and have been successfully applied to analyses of bone loading in a wide range of taxa (Biewener, 1983a; Biewener et al., 1988; Blob and Biewener, 2001; Butcher and Blob, 2008). Studies of energetics have been performed in salamanders based on whole-body force platform data (Reilly et al., 2006), but limb bone loads have not previously been evaluated from isolated footfalls in this clade. Our study will, therefore, allow us to test two specific hypotheses: (1) that salamanders exhibit low limb bone loads and high safety factors, like ectothermic, non-avian reptiles; and (2) that torsion is a prominent loading regime in the salamander femur, as in other species that use sprawling limb posture. Our tests of these hypotheses will improve understanding of limb bone loading mechanics in a previously unstudied clade, and will also provide a better phylogenetic context for interpreting the diversity of limb bone designs in tetrapods.

MATERIALS AND METHODS

Animals

Trials were conducted on five tiger salamanders (three adult females and two adult males, body mass 0.05–0.088 kg, snout–vent length 0.114–0.128 m, total length 0.256–0.289 m) purchased from Charles D. Sullivan Co. (Nashville, TN, USA). Tiger salamanders are aquatic as juveniles, but fully terrestrial as adults (Petranka, 1998). Although they have short limbs with the femur held almost straight out from the body, they are proficient walkers capable of quick bursts when motivated, and generally hold their entire weight off the ground during locomotion (Ashley-Ross, 1994a). Tiger salamanders are also one of the largest species of terrestrial salamanders, making them particularly well suited to the collection of force platform recordings for this study. Salamanders were housed at room temperature (20–23°C) in lidded plastic containers (30.5×30.5×15.0 cm length×width×depth) lined with paper towels that were moistened with aged water and changed daily. The salamanders were fed crickets or worms every other day, and were kept under a 12 h:12 h light:dark cycle. All experimental procedures followed Clemson University IACUC approved guidelines and protocols (AUP 50096). After the completion of force platform data collection, salamanders were euthanized by extended immersion in a buffered solution of tricane methane sulfonate (MS-222, 6 g l^{-1}) and frozen for later dissection and measurement of anatomical variables.

Data collection: three-dimensional kinematics and ground reaction forces

Salamanders were filmed simultaneously in lateral and dorsal views at 100 Hz using two synchronized high-speed digital video cameras (Phantom v.4.1, Vision Research Inc., Wayne, NJ, USA) as they walked across a custom-built force platform (K&N Scientific, Guilford, VT, USA) that was inserted into a wooden trackway (for details, see Butcher and Blob, 2008). An aluminum plate into which a 4×9 cm window had been cut was placed over the 22×17 cm

Table 1. Anatomical data from femora of experimental animals (*Ambystoma tigrinum*)

Measurement	at02	at04	at06	at07	at08
Length (mm)	17.53	14.27	14.65	14.70	15.94
A (mm^2)	1.46	0.85	1.22	1.18	1.20
$r_{c(AP)}$ (mm)	0.06	0.27	0.30	0.54	0.11
$r_{c(DV)}$ (mm)	–0.21	–0.12	–0.36	–0.12	–0.18
y_{AP} (mm)	1.17	1.04	0.63	0.90	0.71
y_{DV} (mm)	1.03	0.87	1.05	0.96	1.03
I_{AP} (mm^4)	0.31	0.11	0.25	0.24	0.31
I_{DV} (mm^4)	0.40	0.14	0.21	0.27	0.29
J (mm^4)	0.71	0.26	0.46	0.50	0.60

Individual animals are identified by alphanumeric codes in the column headings (e.g. at02).

In subscript notations, AP denotes the anatomical anteroposterior direction for the femur; DV denotes the anatomical dorsoventral direction for the femur.

A, cross-sectional area of bone; I, second moment of area; J, polar moment of area; r_c, moment arm due to bone curvature; y, distance from neutral axis to cortex. Curvature sign conventions for AP: positive, concave posterior; negative, concave anterior. Curvature sign conventions for DV: positive, concave ventral; negative, concave dorsal.

surface of the force platform. This window was oriented with its shorter dimension in the direction of travel, and fitted with an aluminum insert that attached directly to the platform surface. This arrangement allowed the recording surface to be restricted to the area of the smaller insert, which increased the likelihood of recording single footfalls. The recording surface of the platform was flush with the trackway, and to prevent slippage or skin abrasion on the feet of the salamanders, the platform was covered with thin rubber and the wood of the trackway was covered with surgical drape.

Salamanders were persuaded to walk by placing an enclosure for them to hide in on the side of the force plate opposite from them and gently squeezing the base of each animal's tail. Successful trials (N=20–26 per animal) consisted of filming a complete isolated footfall of the right hindlimb on the plate with as little overlapping contact on the plate from the right forelimb as possible. Temperature in the trackway was maintained at 20–21.5°C, and salamanders were allowed to rest in aged water between trials to maintain hydration.

Joint and landmark positions (hip, knee, ankle, metatarsophalangeal joint, tip of digit 4 and two body midline points dorsal to the hip) were digitized from both lateral and dorsal AVI video files for each trial using a modification of the public domain NIH Image program for Macintosh (QuickImage, developed by J. Walker; available at http://www.usm.maine.edu/~walker/software.html). Because of difficulty in getting paint markers to adhere to the damp, rubbery skin of salamanders, and concerns about chemical toxicity across their highly permeable skin, landmark locations were tracked by visual inspection of joint centers of rotation during the animation of video frames, aided by distinctive color patches on the animals. For trials with fewer than 40 video frames, every frame was digitized, whereas for trials with 40 or more frames, every second frame was digitized, yielding an effective framing frequency of 50 Hz. The resulting coordinate data files were then calibrated and corrected for parallax using custom programs written in MATLAB (v.7.2.0; The MathWorks Inc., Natick, MA, USA). Data from all traces were then smoothed and normalized to the same duration (101 points) by fitting quintic splines to the traces (Walker, 1998) using QuickSAND software (developed by J. Walker; available at http://www.usm.maine.edu/~walker/software.html).

Our force platform allowed resolution of the ground reaction force (GRF) into vertical, anteroposterior and mediolateral components; specifications of the platform, amplifiers and data-acquisition system were reported in a previous paper (Butcher and Blob, 2008). Force data were collected at 5000 Hz using a custom LabVIEW (v. 6.1; National Instruments, Austin, TX, USA) routine. Amplifier gains were adjusted appropriately for the small body mass of the salamanders to maximize the sensitivity of GRF resolution. Force calibrations were performed daily in all three dimensions, and cross-talk was negligible between force channels. The natural, unloaded frequencies of the platform were 190 Hz in all three directions, sufficiently greater than the stride frequencies of the salamanders (~1 Hz), to avoid confounding the signal produced by the GRF.

To synchronize the force traces with video data, a trigger was pressed during recordings that simultaneously lit an LED visible in the video frame and produced a 1.5 V pulse in the force trace. For the period of foot contact with the plate, each component of the force trace (vertical, anteroposterior and horizontal, calibrated to N) was smoothed and normalized to 101 points (the same number as for kinematic data) using a quintic spline algorithm (Walker, 1998) implemented in QuickSAND software as described previously. Following protocols of previous studies (Blob and Biewener, 2001; Butcher and Blob, 2008), the point of application of the GRF was initially calculated as half the distance between the toe and the ankle; as the heel lifted from the force platform, the point of application was recalculated for each frame as half the distance between the toe and the most posterior part of the foot in contact with the platform. By the end of support, the GRF was applied at the toe, reflecting an anterior shift in the GRF typical during stance phase (Carrier et al., 1994). This approach to evaluating the GRF point of application was used for consistency with previous force-platform studies of sprawling taxa; any error in the assignment of GRF origin should be limited because of the small size of salamander feet.

Steps of the right hindlimb (N~20 per animal) were selected for analysis. Although many trials contained some overlap of the forelimb and hindlimb on the plate at the same time, the trials that were chosen for analysis had a minimal amount of overlap and were as close to isolated footfalls as possible. Animal speed for each trial was calculated ($m\,s^{-1}$) by differentiating the cumulative displacement of a body landmark in QuickSAND, and then normalizing speeds by body length ($BL\,s^{-1}$, with BL defined as total length) for comparisons among individuals. After synchronizing force and limb position data, a custom MATLAB routine was used to calculate GRF components and the joint moments they induce, ultimately allowing evaluation of femoral stresses (see below). Inertial and gravitational moments about the hindlimb joints were assumed to be negligible in our analyses. These are typically small relative to the moments produced by the GRF during stance, and should be particularly so for salamanders in which the limbs are both short and small in mass relative to the body (Alexander, 1974; Biewener, 1983a; Biewener and Full, 1992).

Bone stress analyses

To simplify analyses of stresses in the femur, forces acting on the hindlimbs of salamanders (Fig. 1) were resolved into a frame of reference defined by the anatomical planes of the limb segments following designations for sprawling animals outlined in previous studies (Blob and Biewener, 2001; Butcher and Blob, 2008). Briefly, the anteroposterior (AP) plane was defined as the plane including the long axes of the tibia and femur. The dorsoventral (DV) plane was defined as the plane including the long axis of the femur that is perpendicular to the AP plane. The mediolateral (ML) plane was defined as the plane including the long axis of the tibia that is perpendicular to the AP plane. Thus, the knee and ankle joints flex and extend within the anatomical AP plane. Following this convention, the direction of a motion or force is not the same as the plane in which the motion or force occurs; for example, a dorsally directed force (tending to abduct the femur) would lie within the AP plane rather than the DV plane (Blob and Biewener, 2001).

Details of calculations and equations involved in bone stress analyses closely followed those previously published for reptiles (Blob and Biewener, 2001; Butcher and Blob, 2008). Briefly, femoral stresses were calculated at mid-shaft, where bending moments are typically highest (Biewener and Taylor, 1986), and were derived from free body diagrams of the distal half of the femur (Alexander, 1974; Biewener et al., 1983; Beer and Johnston, 1997). Thus, only forces acting on the distal half of each bone, including the GRF and forces exerted by muscles spanning the mid-shaft of the femur (Fig. 1; Table 2), entered directly into calculations of peak bending stress (Blob and Biewener, 2001; Butcher and Blob, 2008).

To estimate muscle forces, we assumed the limb joints to be in static rotational equilibrium (Alexander, 1974; Biewener, 1983a; Biewener and Full, 1992) and, initially, that the only muscles active at a joint were those that counteract the rotational moment of the

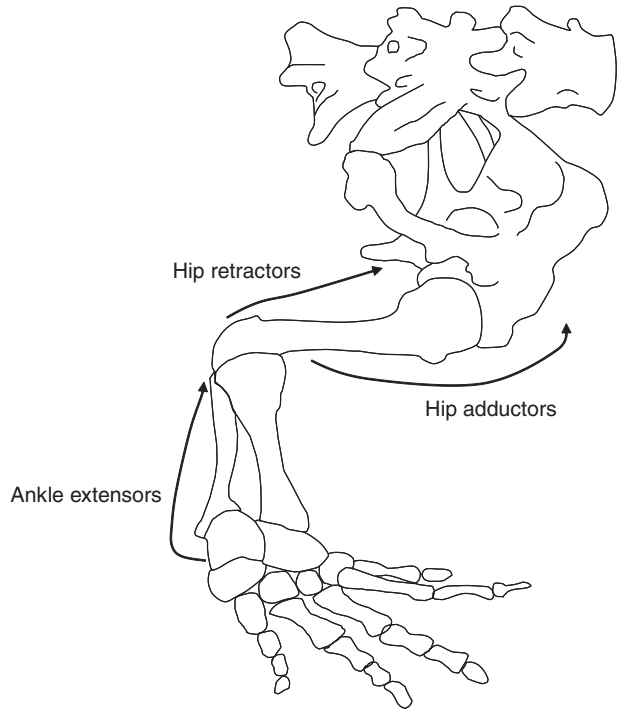

Fig. 1. Sketch (right lateral view) of the hindlimb skeleton of the tiger salamander, *Ambystoma tigrinum*, illustrating the lines of action of the major muscle groups contributing to stresses in the femur during the stance phase of terrestrial locomotion. Rotational forces exerted by the caudofemoralis were not calculated (see Materials and methods).

GRF. With these assumptions, muscle forces (F_m) required to maintain joint equilibrium can be calculated as:

$$F_m = R_{GRF} \times GRF / r_m, \quad (1)$$

where R_{GRF} is the moment arm of the GRF about the joint (calculated in the custom MATLAB routines noted previously) and r_m is the moment arm of the muscles countering the GRF moment (Alexander, 1974; Biewener 1983a; Biewener, 1989). When multiple muscles were active to counteract the GRF moment at a joint, a weighted mean moment arm was calculated for the group based on the physiological cross-sectional areas (PCSA) of each muscle, which are assumed to be proportional to the forces they exert (Alexander, 1974; Biewener and Full, 1992). Muscle moment arms were measured with digital calipers during specimen dissections with the limbs held in a midstance position; PCSAs (Table 2) were calculated following published protocols (Biewener and Full, 1992).

Our model of muscle forces placing stress on the femur included extensors of the ankle, flexors and extensors of the knee, and femoral adductors and retractors (Fig. 1; see Appendix). Because the GRF exerts a flexor moment at the ankle for much of stance (see Results), the ankle extensors were the primary muscles considered at this joint for which forces were evaluated. Anatomical relationships (Ashley et al., 1991; Ashley-Ross, 1992) and electromyographic (EMG) data (Ashley-Ross, 1995) indicate that two muscles are in positions suitable to extend the ankle (i.e. plantarflex the foot): the ischioflexorius (ISF) and the flexor primordialis communis (FPC). Both were considered to be active as ankle extensors in this study.

Evaluating the forces exerted by muscles spanning the femur is complicated because multiple muscle groups cross the hip and knee joints. Details of our model, modified from those previously published for iguanas and alligators (Blob and Biewener, 2001) and turtles (Butcher and Blob, 2008) are presented in the Appendix, but it is based on the following key features: (1) muscles are assumed to act in the same anatomical plane throughout contact; (2) four muscles [caudalipuboischiotibialis (CPIT), caudofemoralis (CDF), iliofemoralis (ILFM) and ISF] are in positions to contribute to retractor moments at the hip, but only the ISF spans the length of the femur (Fig. 1) and is likely to contribute to midshaft femoral stresses; (3) hip adductor muscles [puboischiotibialis (PIT), pubotibialis (PTB) and puboischiofemoralis externus (PIFE)] counter the abductor moment of the GRF at the hip, with all three spanning the midshaft and bending the femur to place its ventral cortex in compression; and (4) neither of the knee extensor muscles on the dorsal aspect of the femur [iliotibialis anterior (ILTA) and posterior (ILTP)] have a consistent, primary phase of activity during stance in salamanders (Ashley-Ross, 1995), so flexor moments at

Table 2. Anatomical data from hindlimb muscles of experimental animals (*A. tigrinum*)

	at02			at04			at06			at07			at08		
Muscle	*A*	θ	r_m	*A*	θ	r_m	*A*	θ	r_m	*A*	θ	r_m	*A*	θ	r_m
Hip retractors															
CPIT	5.2	0	8.5^h	3.6	0	8.6^h	7.0	0	6.2^h	5.2	0	6.6^h	6.0	0	4.2^h
CDF	6.2	0	4.1^h	4.5	0	3.4^h	9.4	0	6.2^h	6.8	0	4.3^h	6.6	0	10.0^h
ILFM	3.8	0	3.6^h	5.7	0	1.3^h	3.5	0	2.2^h	4.2	0	1.4^h	1.1	0	9.9^h
Hip adductors															
PIFE	10.2	15	4.9^h	5.9	10	4.9^h	1.3	10	2.3^h	1.1	15	2.0^h	8.5	15	1.7^h
PIT	11.1	15	3.3^h, 2.6^k	8.2	10	2.4^h, 1.8^k	1.3	10	1.6^h, 2.9^k	1.3	15	0.9^h, 2.9^k	1.3	10	4.0^h, 3.5^k
PTB	2.3	10	2.0^h, 1.8^k	2.1	10	0.9^h, 2.5^k	4.1	10	1.4^h, 1.1^k	5.7	10	1.5^h, 2.3^k	3.6	10	2.1^h, 3.2^k
Ankle extensors															
ISF	1.9	15	7.2^h, 5.1^k, 1.7^a	1.7	15	8.0^h, 2.6^k, 0.8^a	2.4	15	6.8^h, 3.1^k, 2.1^a	2.7	15	8.5^h, 4.2^k, 2.2^a	2.1	10	6.3^h, 6.1^k, 3.0^a
FPC	9.0	0	1.1^k, 1.7^a	5.9	0	0.4^k, 1.0^a	6.3	0	1.7^k, 0.6^a	4.8	0	1.1^k, 1.5^a	8.9	0	0.7^k, 1.3^a

Individual animals are identified as in Table 1.

A, cross-sectional area of muscle (mm^2); θ, angle between the muscle and the long axis of the femur (deg); r_m, moment arm of the muscle (mm) about the joint indicated by the superscript letter (a, ankle; h, hip; k, knee); CPIT, caudopuboischiotibialis; CDF, caudofemoralis; ILFM, iliofemoralis; PIFE, puboischiofemoralis externus; PIT, puboischiotibialis; PTB, pubotibialis; ISF, ischioflexorius; FPC, flexor primordialis communis.

Peak stresses were determined from force platform loading data; *N*=number of steps analyzed.

Values are means ± s.e.m.

the knee must be countered by joint connective tissue and shank muscles originating from the distal femur. As a result, knee extensors were not considered to counter femoral bending induced by the hip adductors, as reptilian models have typically suggested (Blob and Biewener, 2001; Butcher and Blob, 2008). The model we apply in this study thus accounts for known patterns of muscle action to the extent possible. Muscle force calculations were made for each of the 101 time increments for each trial using the custom MATLAB analysis routine.

Muscular contributions to femoral torsion (i.e. shear stresses) were not estimated. The muscle that is likely the primary femoral rotator in salamanders, the caudofemoralis, inserts ventrally on the femur and, thus, would augment the rotational moment imposed by the GRF. Therefore, calculations of the rotational force exerted by this muscle based on equilibrium equations cannot be made without further assumptions about the activity of antagonist muscles. Rather than make such assumptions, the torsional stress induced by the GRF alone was calculated as a minimum estimate (Blob and Biewener, 2001; Butcher and Blob, 2008).

After calculating muscle force estimates, bending moments and axial and bending stresses were calculated following published methods (Biewener, 1983a; Biewener and Full, 1992; Beer and Johnston, 1997), with modifications for three-dimensional analysis (Blob and Biewener, 2001; Butcher and Blob, 2008). Anatomical measurements of linear and angular variables (Table 1) were measured from digital photographs of the femur of each salamander. Cross-sectional anatomical variables (cross-sectional area, second moments of area and polar moment of area; Table 1) were calculated from digital photographs of mid-shaft sections cut from each bone, traced in Microsoft PowerPoint and then input into a custom NIH Image analysis macro (Lieberman et al., 2003). Bending moments and stresses were calculated for perpendicular DV and AP directions (Blob and Biewener, 2001), and accounted for bending induced by axial forces due to the moment arm of bone curvature, r_c (Biewener 1983a; Biewener, 1983b). Net bending stress magnitude at the mid-shaft of the femur was calculated as the vector sum of bending stresses in the DV ($\sigma_{b/DV}$) and AP ($\sigma_{b/AP}$) directions (Blob and Biewener, 2001; Butcher and Blob, 2008), allowing the orientation of peak bending stress to be calculated as:

$$\alpha_{b/net} = \tan^{-1}(\sigma_{b/DV} / \sigma_{b/AP}), \quad (2)$$

where $\alpha_{b/net}$ is the angular deviation of peak stress from the anteroposterior axis. The net neutral axis of bending is perpendicular to the axis of peak stress. Net longitudinal stresses at the points of peak tensile and compressive bending were then calculated as the sum of axial and bending stresses. Torsional stress (τ) due to the GRF was calculated as:

$$\tau = T(y_t / J), \quad (3)$$

where T is the torsional moment applied to the bone by the GRF (determined from the magnitude of the resultant GRF and its orthogonal distance from the long axis of the femur), y_t is the distance from the centroid of the bone to its cortex and J is the polar moment of area (Wainwright et al., 1976). For each animal, y_t was calculated as the mean of the y values from the perpendicular anatomical directions (Table 1).

Mechanical property tests and safety factor calculations

Femora were removed from salamanders during dissection and dried at room temperature for 48–72 h before being embedded in an epoxy plug. Once the plug was dry, it was cut in half through the midshafts of the bones (Buehler IsoMet Low Speed Saw, Lake Bluff, IL, USA). The section of the plug containing the distal halves of the limb bones was polished (Buehler Ecomet III Variable Speed Grinder-Polisher) in preparation for testing of hardness values using a microindenter (Buehler Micromet 5101). The indenter used a diamond tip to make three small indentations in the cortex of each bone. The dimensions of these indentations were then averaged for each individual, and this value was used to calculate the Vickers hardness (H_V) of the bone according to equations provided by the manufacturer. Hardness values were then entered into a linear regression equation (Wilson et al., 2009) derived from data for cortical bone specimens from four taxa from diverse lineages that were reported by Hodgskinson et al. (Hodgskinson et al., 1989). This allowed calculation of tensile yield strength (σ_y):

$$\sigma_y = 32.571 + 2.702\overline{H}_V. \quad (4)$$

This linear equation was used (R^2=0.9), rather than a quadratic equation with a higher R^2 also reported by Wilson et al. (Wilson et al., 2009), because it provided a simpler prediction of the correlation between hardness and tensile yield strength (i.e. there were no first principles reasons to predict a quadratic relationship), and because the quadratic relationship predicted decreasing values of yield strength among the higher values of hardness obtained from bone specimens, for which a mechanical explanation was not apparent. As with any values obtained from a predictive regression, our estimates of tensile yield strength based on converted values of hardness may incur error, but the high R^2 of the regression that we employed indicates that such error was minimized to the extent possible.

To help assess whether data from this species are typical across salamanders, values obtained from tiger salamander femora were supplemented with data obtained from four femora of an additional species of salamander, *Desmognathus quadramaculatus* (Holbrook 1840), supplied by private collectors. *Desmognathus quadramaculatus* also readily walks on land, but spends more time in water than *A. tigrinum* and belongs to a different clade (Plethodontidae, rather than Ambystomatidae) (Petranka, 1998), diversifying the range of salamander taxa for which limb bone mechanical property data are available.

Safety factors for salamander femora were calculated as the ratio of tensile yield stress to the peak tensile locomotor stress. Mean safety factors were calculated using the mean values for peak yield stress and peak locomotor stress across all individuals. 'Worst-case' safety factors were calculated using the mean yield stress minus two standard deviations and the mean peak tensile stress plus two standard deviations (Blob and Biewener, 1999; Blob and Biewener, 2001; Butcher and Blob, 2008).

Mean values are presented ±s.e.m.

RESULTS

Overview of stance phase kinematics

Tiger salamanders use a diagonal-couplet, lateral sequence walk (Hildebrand, 1975; Ashley-Ross, 1994a). Salamander hindlimb kinematics have been described in detail for another highly terrestrial species, *Dicamptodon tenebrosus* (Ashley-Ross, 1994a), and will be summarized only briefly here for *A. tigrinum* (walking at 0.126±0.005 m s^{-1}, 0.45±0.02 BL^{-1}). At the beginning of stance, the femur is oriented near parallel to the ground (defined as 0 deg) with the hip slightly adducted (–12±1 deg; Fig. 2). The femur is also in a protracted position at the beginning of stance (23±5 deg, where 0 deg is perpendicular to the long axis of the body) whereas the proximal tibia is oriented posteriorly (i.e. knee posterior to ankle) by –33±1 deg (vertical=0 deg) and medially by –37±1 deg

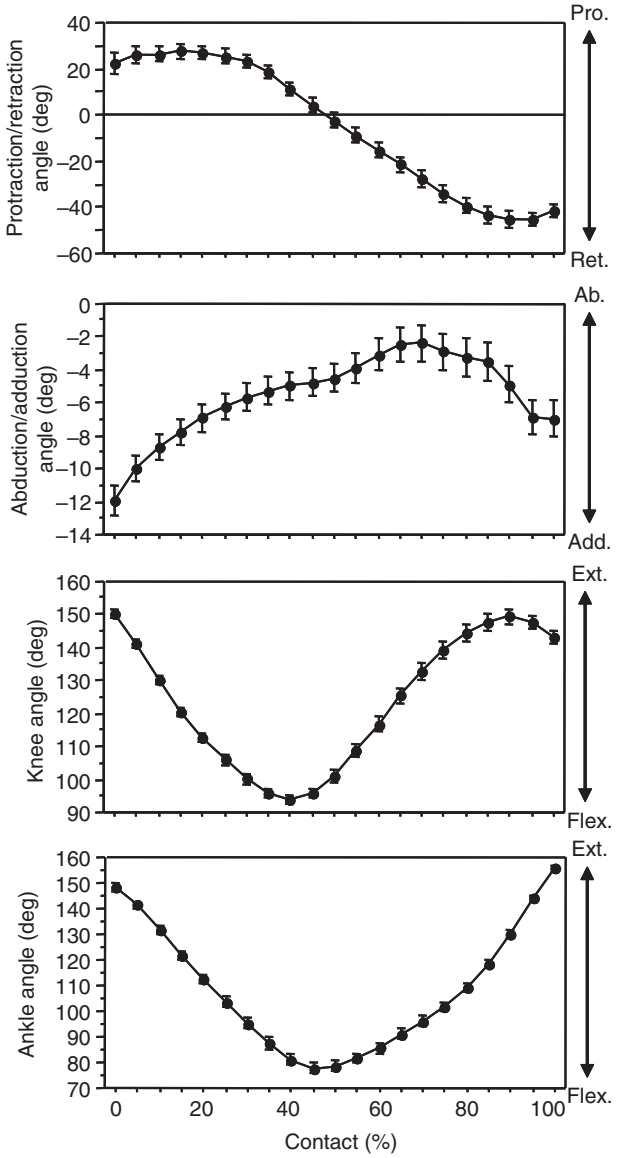

Fig. 2. Representative kinematic profiles of right hindlimb joints for tiger salamanders during a walking step over a force platform. Top to bottom: femoral (hip) protraction (Pro.)/retraction (Ret.) angle, femoral (hip) abduction (Ab.)/adduction (Add.) angle, knee angle and ankle angle (Ext., extension; Flex., flexion). Kinematic profiles represent mean ± s.e.m. angles averaged across all five salamanders (*N*=20–26 trials per individual, 118 total steps per data point). Note that *y*-axis scales differ for these plots to provide increased resolution for smaller angles.

(vertical=0 deg). Foot posture is plantigrade, with the digits pointing forward or slightly laterally. The femur retracts through a range of nearly 70 deg during stance. It is also abducted by approximately 10 deg to an essentially horizontal orientation by midstance before adducting nearly back to its starting position by the end of stance (Fig. 2). The knee and ankle joints initially flex as they begin supporting the weight of the body during stance, but then re-extend as the salamander pushes off the substrate (Fig. 2), causing the tibia to approach a nearly horizontal (90 deg) AP orientation.

GRF magnitude and orientation

The GRF is oriented upward, anteriorly and medially throughout almost all of stance phase, with the vertical component considerably larger in magnitude than both the AP and ML components (Fig. 3). The net GRF reaches peak magnitude just over a quarter of the way through the stance (pooled mean: 33.4±1.5%; Table 3). Peak net GRF magnitude averaged 0.50±0.01 BW across all five salamanders, with an essentially vertical orientation through the middle 20–40% of the contact interval (pooled mean at peak net GRF: AP angle, 13.5±1.6 deg; ML angle, –7.6±0.7 deg; 0 deg=vertical in both directions, with positive values indicating anterior and lateral inclinations; Table 3; Fig. 3B,C).

The femur begins the step in a protracted and depressed position. Similar to patterns described in reptiles (e.g. Butcher and Blob, 2008), the hip joint moves anteriorly as the femur is retracted throughout the contact interval and the femur moves anteriorly relative to the foot. Because of the protracted initial orientation of the femur and the lateral placement of the foot, the nearly vertical net GRF vector is disposed posterior to the long axis of the femur for much of stance (Fig. 3). Because of this vertical GRF orientation and the nearly horizontal orientation of the femur (Fig. 2), the net GRF vector is directed at almost a right angle to the femur for most of the step, increasing to a mean of 98.1±1.5 deg across all five salamanders at peak net GRF magnitude (Table 3). Considering the near vertical orientation of the GRF vector and rotation of the femur about its long axis (counterclockwise when viewing the right femur from its proximal end; Fig. 4), femoral bending that is initially DV (i.e. about an axis close to the anatomical AP axis, with the neutral axis <45 deg from AP) would shift toward AP bending (i.e. about an axis close to the anatomical DV axis) over the course of the step.

Moments of the GRF about hindlimb joints

The GRF exerts moments in a consistent direction throughout stance for most hindlimb joints. Because of its position anterior to the ankle, the GRF tends to dorsiflex the ankle for nearly all of stance phase, except at the very end as the foot is lifted from the ground (Fig. 4). To counter this moment, ankle extensor muscles would need to be active. Similarly, the GRF exerts a knee flexor moment at the knee for nearly all of stance, reaching a maximum at approximately 20% of the contact interval (Fig. 4). The upward orientation of the GRF also leads to a consistent abductor moment at the hip that increases rapidly after toe-down and reaches a maximum at 20–30% stance (Fig. 4). This moment would require activity by femoral adductors to maintain equilibrium. Patterns for the AP moment at the hip differ somewhat from the others described, as there is a shift from an early retractor moment to a protractor moment later in stance (Fig. 4). However, this moment is at its lowest magnitude when the GRF is at its peak between 20 and 40% of stance (Figs 3, 4).

The GRF also exerts torsional moments on the femur (Fig. 4). As the GRF initially acts posterior to the long axis of the femur during stance, it exerts a moment that rotates the long axis of the femur anteriorly or inwardly (i.e. counterclockwise if viewing the right femur from its proximal end). However, like the anteroposterior moment at the hip, this moment changes direction as the hip moves over the foot and the femur retracts during stance. Torsional moments increase to a maximum at between 25 and 35% of the contact interval, similar to the timing of maximal hip abductor and knee flexor moments. After this maximum, the torsional moment decreases until approximately 90% stance, at which point the GRF exerts a rotational moment on the femur in the opposite direction (i.e. clockwise if viewing the right femur from its proximal end; Fig. 4).

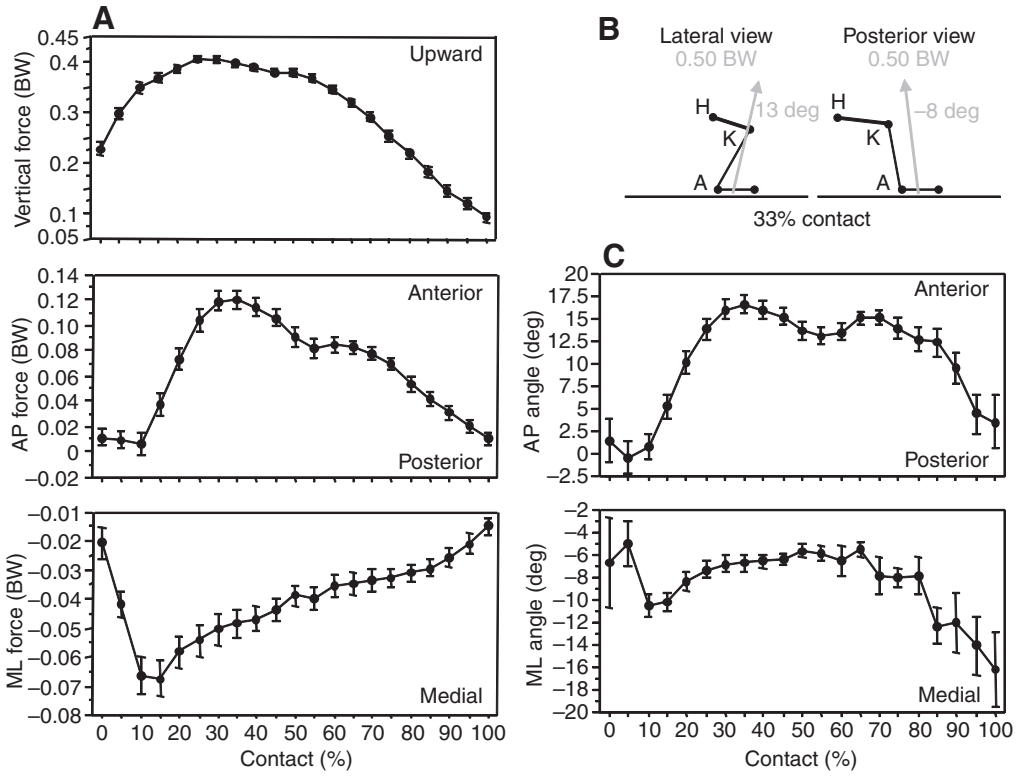

Fig. 3. Mean ground reaction force (GRF) dynamics for the right hindlimb of tiger salamanders. All plots show means ± s.e.m. averaged across all five salamanders (*N*=20–26 trials per individual, 118 total steps per data point). (A) Vertical, anteroposterior (AP) and mediolateral (ML) GRF components in body weight (BW), with positive values indicating upward, anterior and lateral forces, respectively. *y*-axis scales differ for these plots to provide increased resolution for the small AP and ML forces. All trials were normalized to the same duration, allowing values to be graphed against the percentage of time through the stance. (B) Limb segment positions at the mean time of peak net GRF (33% contact) during a representative step by *A. tigrinum*, with the direction and magnitude of the GRF vector illustrated. The femur is highlighted by bold lines; note that it is foreshortened in lateral view. A, ankle; H, hip; K, knee. (C) AP and ML orientations of the net GRF vector. AP angles were determined relative to vertical at 0 deg (90 deg indicates GRF horizontal, pointing forward; <0 deg indicates posteriorly directed GRF). ML angles were determined relative to vertical at 0 deg (negative values indicate medially directed GRF).

Femoral stresses

Because of the large moments exerted by the GRF in the abductor direction at the hip, as well as about the other hindlimb joints, hindlimb muscles appear to exert large forces that make substantial contributions to DV bending stresses in the femur (Fig. 5). Contraction of the adductor muscles and the external action of the GRF exert DV bending stresses on the femur in opposite directions. In contrast, among retractor muscles, only the ischioflexorius spans the length of the femur and is likely to contribute directly to femoral stress (see Appendix); however, because it represents only a small fraction of the total physiological cross-sectional area of the retractors (12.1±0.7%; Table 2), it exerts little force and imposes minimal AP bending stress. Bending stresses induced by the axial component of the GRF are also quite small and have little consequence for overall loading patterns of the limb.

The femur of *A. tigrinum* is exposed to a combination of axial compression, bending and torsion. Maximum tensile and compressive stresses occurred nearly simultaneously during each

Table 3. Mean ground reaction force (GRF) parameters for *A. tigrinum* at the time of peak net GRF

	GRF							
Individual	Vertical (BW)	AP (BW)	ML (BW)	Peak net GRF time (%)	Net GRF (BW)	GRF femur angle (deg)	GRF AP angle (deg)	GRF ML angle (deg)
at02 (*N*=25)	0.43±0.01	0.13±0.02	–0.04±0.02	32.5±3.1	0.47±0.01	93.2±3.0	16.7±2.4	–5.0±2.4
at04 (*N*=20)	0.53±0.02	–0.02±0.04	–0.11±0.01	34.9±4.1	0.58±0.02	105.7±2.7	–0.5±4.1	–11.9±1.2
at06 (*N*=23)	0.45±0.01	0.06±0.04	–0.06±0.01	35.1±3.6	0.49±0.01	101.4±2.7	7.7±4.4	–7.7±1.6
at07 (*N*=24)	0.47±0.01	0.11±0.02	–0.05±0.01	36.4±4.0	0.49±0.02	107.3±2.4	13.1±2.4	–6.5±1.1
at08 (*N*=26)	0.44±0.01	0.23±0.02	–0.06±0.01	28.8±2.0	0.50±0.01	85.5±3.3	26.9±1.6	–7.7±1.2
Mean	0.46±0.01	0.11±0.01	–0.06±0.01	33.4±1.5	0.50±0.01	98.1±1.5	13.5±1.6	–7.6±0.7

GRF femur, angle of ground reaction force to the femur; GRF AP, anteroposterior inclination angle of GRF; GRF ML, mediolateral inclination angle of GRF.
Vertical=0 deg for GRF AP and ML angles of inclination; for GRF AP, negative angles are posteriorly directed and positive angles are anteriorly directed; for GRF ML, negative angles are medially directed.
BW, body weight.
Values are means ± s.e.m. (*N*=number of steps analyzed).

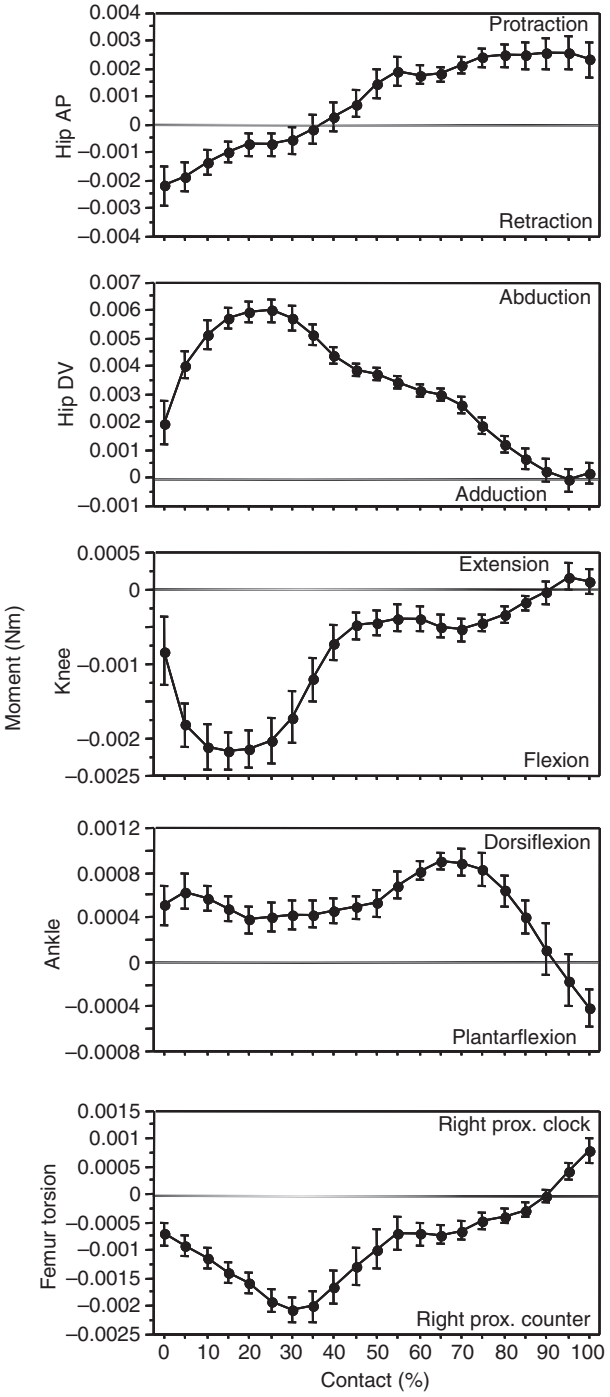

Fig. 4. Moments exerted by the GRF about the hindlimb joints and the long axis of the femur from an individual salamander. All plots show means ± s.e.m. over *N*=18 trials. Note that *y*-axis scales differ for these plots to provide greater resolution for smaller moments. Directions of moments are labeled to the right of the figure plots. Hip AP, the GRF moment about the hip in the anatomical anterior and posterior directions; Hip DV, the GRF moment about the hip in the anatomical dorsal and ventral directions; Right prox. clock., torsional GRF moment, clockwise when viewing the right femur from the proximal end; right prox. counter., torsional GRF moment, counterclockwise when viewing the right femur from its proximal end.

step (Table 4, Fig. 6). The timing of peak stress varied among individuals, but generally occurred prior to midstance, just in advance of the peak magnitude of the net GRF (at a net GRF

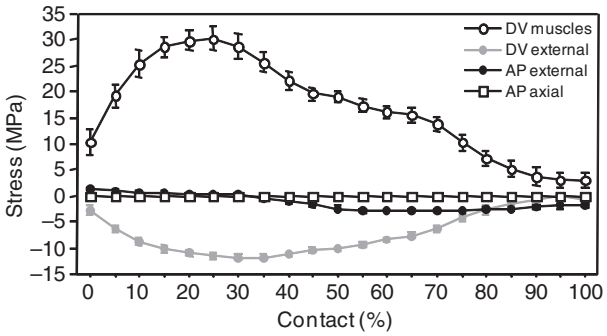

Fig. 5. Components of bending stress in the femur induced by muscles and GRF components from an individual salamander. All data are mean ± s.e.m. stresses over *N*=18 trials. Stresses plotted are those occurring on the dorsal surface for forces acting to cause dorsoventral (DV) bending, and those occurring on the anterior surface for forces acting to cause AP bending. Tensile stress is positive and compressive stress is negative. 'Muscles' indicates stresses induced by major muscle groups in the direction indicated; 'external' indicates stresses induced by the GRF acting in the direction indicated; 'axial' indicates stresses induced by the axial component of the GRF due to bone curvature in the direction indicated. AP bending stresses induced by muscles (i.e. ischioflexorius) and both AP and DV bending stresses induced by axial forces are very small and overlap along the zero line. For clarity, only stresses induced by AP axial forces are plotted.

magnitude of 0.42 BW *versus* the peak net GRF at 0.50 BW), when the GRF vector was oriented nearly vertically (Table 4; Fig. 6). The net plane of bending (i.e. angle of the neutral axis from the anatomical AP axis) shifts over the course of the step, reflecting axial rotation of the femur, but at the time of peak tensile stress (pooled mean: 29.8±2.0% contact) tended to place the anatomical 'posterodorsal' cortex in tension and the 'anteroventral' cortex in compression (Fig. 6). This distribution of loading reflects the dominance of adductor muscles and limited activity of dorsally situated knee extensors (Ashley-Ross, 1995) in our model (Fig. 5; see Appendix). Because the GRF is near vertical for most of stance, shifting of the neutral axis indicates maintenance of a similar absolute direction of bending through the step.

Peak tensile and compressive stresses averaged 14.9±0.8 and –18.9±1.0 MPa, respectively, across all five salamanders, with no clear correlation with speed across the limited range used by the animals in our study. Peak compressive stresses are greater than peak tensile stresses (Table 4) because axial compression (–1.9±0.1 MPa) is superimposed on bending during stance. Peak femoral shear stresses averaged 4.1±0.3 MPa across all five salamanders and typically occurred later during stance (41.5±2.8% contact) than peak bending stresses (Table 4). As noted in the Materials and methods, these values (like those calculated for the species noted above) are minimum estimates that do not account for torsion produced by limb muscles, but instead reflect the rotational moment exerted by the GRF on salamander femora, tending to produce inward rotation during stance.

Material properties and safety factor calculations

Hardness values for femora from *A. tigrinum* and *D. quadramaculatus* (46.4±1.4 and 45.3±1.3, respectively; Table 5) were extremely similar, and produced nearly identical estimates of yield stress (157.1±3.7 and 154.9±3.6 MPa, respectively) that were very similar to previous evaluations of bending strength for *A. tigrinum* (149±50.2 MPa) (Erickson et al., 2002). Based on data from

Table 4. Mean peak stresses for femora of *A. tigrinum* with GRF magnitudes and orientations at peak tensile stress

		Peak stress							Neutral axis				
Individual	*N*	Tensile (MPa)	Comp. (MPa)	Axial (MPa)	Shear (MPa)	Peak tens. time (%)	Peak comp. time (%)	Peak shear time (%)	angle from AP (deg)	Net GRF (BW)	GRF AP angle (deg)	GRF ML angle (deg)	Speed (BL s^{-1})
at02	25	8.2±0.4	–10.6±0.6	–1.2±0.1	3.3±0.2	29.2±5.3	26.4±4.9	28.8±3.8	–33.9±7.1	0.41±0.01	10.0±2.3	–5.0±2.5	0.47±0.02
at04	20	12.2±1.0	–14.1±0.9	–0.8±0.1	6.4±0.9	55.6±3.0	42.4±5.1	32.8±4.8	–37.4±14.5	0.49±0.03	3.1±3.7	–10.2±1.0	0.71±0.04
at06	23	19.9±1.4	–24.9±1.6	–2.1±0.2	5.2±0.4	20.2±3.8	22.1±3.4	40.4±7.3	–3.4±2.5	0.34±0.03	0.9±4.4	0.1±7.4	0.48±0.02
at07	24	26.3±1.8	–33.4±2.2	–3.5±0.2	3.4±0.7	21.8±1.9	22.5±1.7	53.9±7.0	–8.9±2.1	0.44±0.01	11.7±1.7	–6.3±1.6	0.44±0.02
at08	26	8.3±0.8	–11.8±1.0	–1.7±0.2	2.7±0.2	26.3±3.1	22.4±2.3	50.4±6.4	–13.7±6.2	0.43±0.02	23.7±1.7	–7.3±1.4	0.23±0.04
Mean ± s.e.m.	118	14.9±0.8	–18.9±1.0	–1.9±0.1	4.1±0.3	29.8±2.0	26.6±1.7	41.5±2.8	–19.0±3.4	0.42±0.01	10.4±1.5	–5.6±1.6	0.45±0.02

Shear stresses are reported for counterclockwise rotations of the right femur as viewed from the proximal end. Axial stresses are reported at the time of peak tensile stress. Peak tension (tens.) and compression (comp.) time are shown as a percentage of stance.

Deviations of the neutral axis from the anatomical AP axis of each bone are clockwise in direction (i.e. negative angle from horizontal at 0 deg); use of this negative angle convention rather than those of our previous papers (Butcher and Blob, 2008; Butcher et al., 2008) allows continuous plotting of values in Fig. 6 (e.g. a value of –10 deg in this paper would be equivalent to a value of 170 deg in the cited studies).

BL, body length.

Vertical=0 deg for GRF AP and ML angles of inclination; for GRF AP, negative angles are posteriorly directed and positive angles are anteriorly directed; for GRF ML, negative angles are medially directed and positive angles are laterally directed.

A. tigrinum, the mean femoral safety factor in bending was calculated as 10.5 with a worst-case estimate of 4.5 (Table 5). Femoral safety factor values in bending are generally higher than those determined for alligators and iguanas [mean: 6.7–8.0; worst-case: 4.5–3.2 (Blob and Biewener, 2001)], whereas turtles have a higher mean estimate (13.9) but lower worst-case estimate (2.8) (Butcher and Blob, 2008).

DISCUSSION

Loading regimes and magnitudes in salamander femora

Findings from salamanders confirm broad patterns that have emerged from studies of bone loading across tetrapod lineages. Like other sprawling tetrapods in which limb bone loading has been evaluated [iguanas and alligators (Blob and Biewener, 1999; Blob

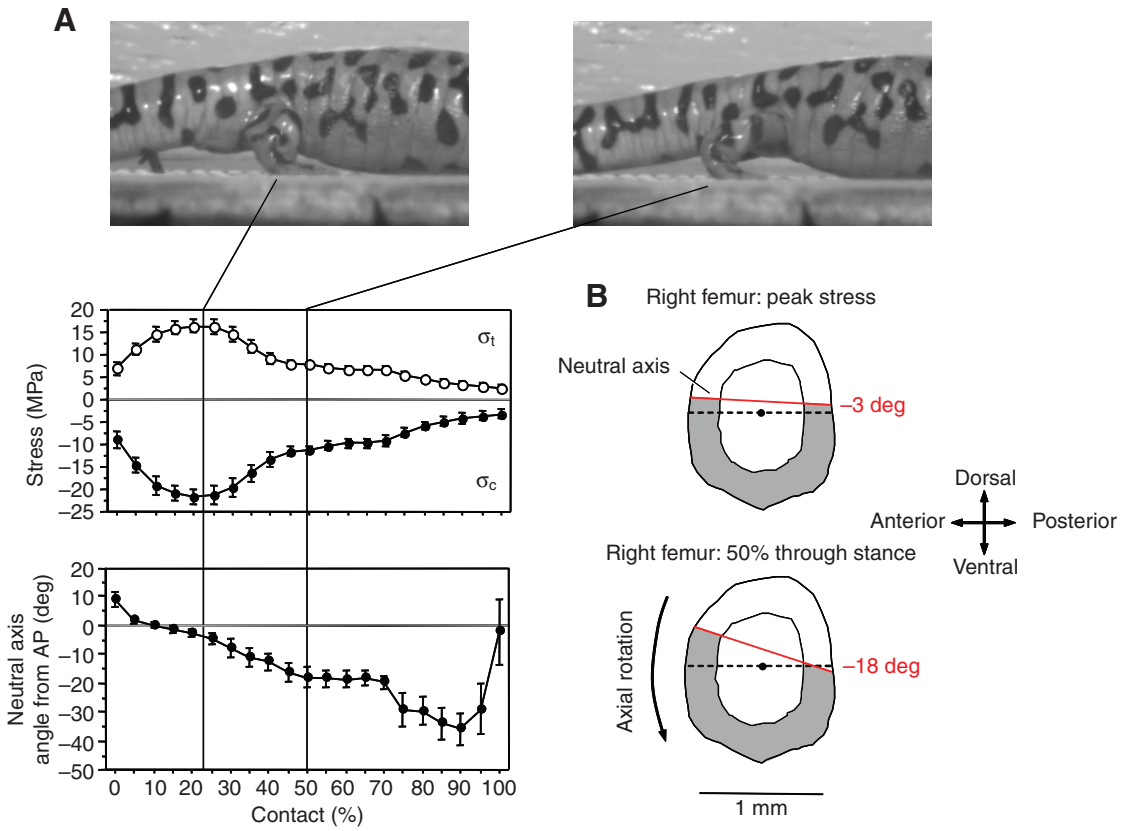

Fig. 6. (A) Maximum tensile (σ_t, open circles) and compressive (σ_c, filled circles) stresses acting in the right femur and neutral axis angle from the anatomical AP axis of the femur from an individual salamander. Plots show means ± s.e.m. over *N*=18 trials. Frame stills show limb position at the time of maximum tensile stress (left image) and at 50% of the way through stance (right image). Solid vertical lines mark the relative timing of these events. (B) Schematic cross-sections of a right femur illustrating neutral axis orientations for bending (red line and values) at peak tensile stress (upper) and 50% of the way through stance (lower), matching the time of the second image shown in A. Neutral axis is illustrated offset from the centroid (dark circle) because of axial compression superimposed on bending loads. Mean rotation of the neutral axis over the course of a walking step indicates that the 'anteroventral' cortex of the femur experiences compression (shaded) and the 'posterodorsal' cortex experiences tension (unshaded). The curved arrow (black) indicates the inward rotation of the femur during a step.

Table 5. Mechanical properties and safety factors for salamander femora

	Ambystoma tigrinum	*Desmognathus quadramaculatus*
N	5	4
Hardness	46.1±1.4	45.3±1.3
Yield stress (MPa)	157.1±3.7	154.9±3.6
Safety factor mean	10.5	–

Safety factors are calculated based on functional stresses measured for *A. tigrinum* only, see Table 4.
Values are means ± s.e.m.

and Biewener, 2001); turtles (Butcher and Blob, 2008; Butcher et al., 2008)], salamander femora are exposed to considerable torsion as well as a combination of axial compression and bending. These loading regimes result from forces and moments imposed by both limb muscles and the GRF. The GRF has a nearly vertical orientation for much of the step in salamanders, including the time of peak femoral stress when the mean medial inclination angle of the GRF is only 5.6 deg (Table 4). This GRF orientation is similar to that seen in other sprawling tetrapods, in which medial inclinations typically range between 3 and 13 deg (Jayes and Alexander, 1980; Blob and Biewener, 2001; Butcher and Blob, 2008), as well as that seen in many mammals that use parasagittal limb posture (Biewener et al., 1983; Biewener et al., 1988). As a consequence of this GRF orientation and their sprawling limb posture, the salamander femur is nearly orthogonal to the GRF at the time of peak loading (98.1±1.5 deg; Table 3), maximizing bending moments and stresses relative to those induced by axial forces (Fig. 5).

The morphology, locomotor behavior and phylogenetic relationships of salamanders led to alternative predictions about the magnitudes of femoral stresses that they might encounter. Given the small diameter of salamander femora compared with the mass of the body, locomotor forces might be imposed on femora that are not very robust, leading to high femoral stresses. However, our results indicate low levels of bending stress in salamander limb bones (14.9±0.8 MPa in tension, –18.9±1.0 MPa in compression; Table 4). These values are close to those reported for sprawling reptiles [e.g. alligators: 11.7±0.6 and –16.4±0.9 MPa; iguanas: 27.1±2.1 and –37.0±2.8 MPa; river cooter turtles: 24.9±1.0 and –31.1±1.0 MPa (Blob and Biewener, 2001; Butcher and Blob, 2008)], but lower than values typically calculated for birds and mammals [e.g. –25 to –74 MPa for the femur in compression (Biewener, 1991)]. One factor likely contributing to the low femoral stresses of tiger salamanders is that they do not generally use a kinematic running gait (Reilly et al., 2006) and have three feet on the ground for more than half of stance (Ashley-Ross, 1994a). Another factor that may lower stresses on salamander femora is their relatively short limb bones, because bending moments applied by forces acting transverse to a limb bone are directly proportional to the length of that bone (Alexander, 1974; Wainwright et al., 1976; Biewener, 1983a; Blob and Biewener, 2001). Although lizards of similar body mass to our salamanders would be predicted to have femora 28.45 mm long [based on regression data from Blob (Blob, 2000)], the femora of our salamanders averaged only 15.42 mm in length (Table 1). Although the short limbs of salamanders may represent the retention of an ancestral condition, or an adaptation to functional demands unrelated to bone loading, lowering of bone stress may, nonetheless, be a consequence of this morphological design.

As in other sprawling lineages in which bone loading has been evaluated, the GRF imposes significant torsion in salamander femora (4.1±0.3 MPa, Table 4). The inward rotational moment imposed on salamander femora by the GRF would likely be augmented by inward rotation imposed by the caudofemoralis muscle during limb retraction, further elevating torsional stress. The GRF also imposes an inward rotational moment on the femur in turtles (Butcher and Blob, 2008), but generates much higher shear stresses (13.7±0.5 MPa) than in salamanders. Although previous studies had predicted that elevated torsion would be expected in species that drag a large tail on the ground behind the legs (Reilly et al., 2005), the high level of torsion in turtles, in which the tail is reduced, indicates that tail dragging in and of itself is not the sole factor inducing femoral torsion in sprawling taxa (Butcher and Bob, 2008; Butcher et al., 2008). However, along with the smaller size of the tail, caudofemoral musculature is also reduced in turtles (Walker, 1973; Blob et al., 2008) and may make only limited contributions to their femoral shear stress. With the muscular augmentation of femoral shear stress expected in salamanders, it is possible that their net femoral shear stresses may approach the high levels seen in turtles.

Safety factors in salamander femora: mechanical basis and evolutionary implications

Safety factors determined for the femora of tiger salamanders were 10.5 in bending, approaching the magnitudes of estimates from force-platform-based evaluations for river cooter turtles [13.9 (Butcher and Blob, 2008)], but considerably higher than values previously reported for mammals (Alexander, 1981; Biewener, 1983a; Biewener, 1993), and potentially also higher than safety factors of reptilian taxa such as iguanas and alligators (Blob and Biewener, 2001). However, in contrast to turtles (Butcher and Blob, 2008), the high femoral safety factors observed in salamanders appear to result primarily from low peak locomotor stresses rather than elevated bone yield strengths. We tested bone material properties for the femora of two different salamander species, *A. tigrinum* and *D. quadramaculatus*, that exhibit very different habits. *Ambystoma tigrinum* are large-bodied salamanders that spend considerable time walking over land, whereas *D. quadramaculatus* are slender, primarily aquatic salamanders that live in cold streams (Petranka, 1998). These two species showed very similar femoral yield stresses (*A. tigrinum*, 157.1±3.7 MPa; *D. quadramaculatus*, 154.9±3.6 MPa), suggesting that these values could be broadly representative for the salamander lineage. These values are not, however, especially distinctive compared with data from other tetrapod femora (Currey, 1987; Erickson et al., 2002), indicating that the high safety factors of tiger salamander limb bones result primarily because this species simply incurs low stress magnitudes during locomotion.

The high safety factors observed in salamander femora might help to accommodate variability in femoral stresses or the ability to resist stress (Lowell, 1985; Blob and Biewener, 1999; Blob and Biewener, 2001; Butcher and Blob, 2008). Seasonal variation in bone material properties seems less likely for salamanders than it might be for reptilian lineages with high safety factors, as amphibians do not produce highly calcified egg shells that may require resorption of limb bone minerals (Edgren, 1960; Suzuki, 1963; Wink and Elsey, 1986). However, the peak loads experienced by salamander femora are fairly variable: coefficients of variation for peak tensile stress and shear stress in our salamanders averaged 35 and 54%, respectively, similar to values reported for reptiles with high limb bone safety factors [37–80% in alligators, 14–50% in iguanas (Blob and Biewener, 1999); 31–33% in turtles (Butcher and Blob, 2008)], but much higher than the 8% coefficient of variation for limb bone

stresses seen in birds and mammals during terrestrial locomotion (Biewener, 1991). High limb bone safety factors in salamanders might also help to safeguard against load variability resulting from non-locomotor activities that salamanders perform with their limbs, such as burrowing or mating, though the magnitudes of such loads have yet to be evaluated.

Although natural selection has often been invoked as a regulator of safety factors by selecting against those that are costly to maintain or provide inadequate protection (Alexander, 1981; Lanyon, 1991; Diamond and Hammond, 1992; Diamond, 1998), the possibility that natural selection has acted to optimize safety factors across lineages facing different demands should be viewed with caution (Garland, 1998). For example, amphibians and non-avian reptiles might show higher limb bone safety factors than birds and mammals simply as an emergent consequence of meeting other functional demands (Butcher and Blob, 2008; Butcher et al., 2008). Alternatively, high limb bone safety factors in some lineages might indicate the retention of an ancestral condition that was not sufficiently disadvantageous to be selected against (Blob and Biewener, 1999; Butcher and Blob, 2008). Our data from *A. tigrinum* support this latter conclusion because of the phylogenetic position of salamanders as an outgroup to amniotes (Gao and Shubin, 2001). However, specific comparison of our data from salamanders and previous studies of turtles (Butcher and Blob, 2008; Butcher et al., 2008) also indicates that there may be more than one path to high limb bone safety factors (e.g. low limb bone loads, high bone strength or a combination of the two), further demonstrating that the diversity of tetrapod limb bone loading patterns is more extensive than studies of animals with upright posture had suggested. The presence of multiple pathways to high femoral safety factors also draws parallels to the 'many-to-one mapping' of structure to function documented in a range of vertebrate systems (Alfaro et al., 2005; Wainwright et al., 2005; Blob et al., 2006). Examination of bone loading mechanics in other functionally distinct or phylogenetically unsampled clades will help to document the extent of diversity in limb bone loading, and provide insight into the factors that have influenced the evolution of limb design across tetrapods.

APPENDIX

In the AP direction, four main muscles are in anatomical positions suitable to act as primary femoral retractors during stance in tiger salamanders: the CPIT, the CDF, the ILFM and the ISF (Ashley et al., 1991; Ashley-Ross, 1992). EMG data verify activity during limb retraction for the CPIT, the CDF and the ISF in closely related Pacific giant salamanders (*Dicamptodon tenebrosus*) (Ashley-Ross, 1995). In our model, all four muscles were considered capable of generating force to oppose protractor moments induced by the GRF. However, of these muscles, only the ISF was considered to potentially contribute directly to midshaft stresses because it is the only muscle of these four that spans the femoral midshaft (Ashley et al., 1991; Ashley-Ross, 1992).

Forces acting on the femur in the DV direction are exerted by muscles that span the hip and knee. Previous anatomical analyses (Ashley et al., 1991; Ashley-Ross, 1992) and our own dissections indicate that three major muscles situated along the ventral aspect of the femur could act as adductors to counter the abductor moment exerted by the GRF through most of stance: the PIT, the PTB and the PIFE. EMG data verify stance-phase activity during limb retraction for all three of these muscles in Pacific giant salamanders (Ashley-Ross, 1995). Because all three of these muscles also span the femoral midshaft in salamanders, they were all considered to contribute to femoral stress.

The GRF also exerts flexor moments at the ankle and knee for much of stance. Flexor moments at the ankle are opposed by the action of two ankle extensor muscles, the ISF and the FPC, for which EMG data indicate stance phase activity in salamanders (Ashley-Ross, 1995). Both the ISF and the FPC cross the knee joint, augmenting the flexor moment of the GRF and suggesting that knee extensors on the anatomical dorsal surface of the femur could act to counter this knee flexor moment, bending the femur dorsally in opposition to the femoral adductors. Muscles situated in anatomical positions to extend the knee include the ILTA and the ILTP, running from the hip distally to the knee, and the extensor digitorum communis (EDC) and extensor tibialis (EXT), running from the shank proximally to the knee. Of these, only the ILTA and the ILTP span the femoral midshaft, but EMG data from *D. tenebrosus* indicate that the ILTA is not active during stance, and the ILTP has only variable, secondary bursts of activity during stance (Ashley-Ross, 1995). As a result, a simplifying assumption was made that knee extensors spanning the femoral midshaft were not active during stance, and that knee flexor moments induced by the GRF and ankle extensors would be accommodated by joint connective tissue and shank muscles spanning the extensor surface of the knee (EDC and EXT). Although this approach does not consider potential effects of the dorsal thigh muscles to counter femoral bending induced by femoral adductors, effects on stress calculations should be minimized because EDC and EXT do not span the femoral midshaft, and ILTP (the muscle for which potential activity is being neglected) accounts for less than half of the cross-sectional area (and likely force generating capacity) of the dorsal thigh muscles (Ashley et al., 1991) (dissection data from this study).

To account for known co-activation of muscle groups and other complications to the extent possible, we modeled the force production of muscles spanning the knee and hip in tiger salamanders as follows, using approaches generally similar to those of Blob and Biewener (Blob and Biewener, 2001) and Butcher and Blob (Butcher and Blob, 2008), but with modifications appropriate for salamanders as required. First, muscle groups were assumed to act in the same anatomical plane throughout stance. Although this is a potential source of error in force calculations for some muscles originating from the hip, it is likely reasonable for most major muscles such as the adductors, for which portions on the protractor and retractor sides of the hip joint are approximately equivalent. This rule was modified for the retractor ISF, for which the capacity to flex the knee was considered despite a disposition primarily on the posterior (rather than ventral) aspect of the femur. Second, the force exerted by hindlimb retractors was calculated as that necessary to counter the protractor moment of the GRF. Third, the force exerted by hip adductors was calculated as that necessary to maintain equilibrium with the abductor moment of the GRF at the hip. This approach may underestimate adductor force because it does not account for a possible abductor moment of ILTP at the hip; however, this effect is likely minimal because stance phase activity of ILTP is not consistent, and because ILTP accounts for less than half of cross-sectional area of the dorsal thigh muscles (Ashley et al., 1991). And fourth, knee flexor moments of the GRF were augmented by femoral retractors and ankle extensors, but were countered by joint connective tissue and the action of shank muscles crossing the extensor surface of the knee to the distal femur, neither of which contribute to femoral bending stress.

In some trials, muscle forces calculated for the knee extensors were extremely high and would have resulted in unreasonable muscle stresses. Maximum isometric stresses of amphibian limb muscles can exceed 250 kPa (Lutz and Rome, 1994; Lutz and Rome,

1996; Peplowski and Marsh, 1997; Kargo and Rome, 2002; Roberts and Marsh, 2003), though muscle stresses can be as much as 80% greater than maximum isometric stress during lengthening contractions (Cavagna and Citterio, 1974; Flitney and Hirst, 1978). To accommodate the possibility of such conditions, we made a final assumption in our model that prevented calculated muscle forces from exceeding values that could produce muscle stresses over 390 kPa (Butcher and Blob, 2008).

LIST OF ABBREVIATIONS

AP	anteroposterior
CDF	caudofemoralis
CPIT	caudalipuboischiotibialis
EDC	extensor digitorum communis
EXT	extensor tibialis
EMG	electromyographic
DV	dorsoventral
FPC	flexor primordialis communis
GRF	ground reaction force
ILFM	iliofemoralis
ILTA	iliotibialis anterior
ILTP	iliotibialis posterior
ISF	ischioflexorius
ML	mediolateral
PIFE	puboischiofemoralis externus
PIT	puboischiotibialis
PTB	pubotibialis

ACKNOWLEDGEMENTS

We thank K. Shugart, A. Sheffield and M. Butcher for assistance with data collection and analysis; G. Rivera for construction of the trackway; and S. Cirilo, S. Gosnell, T. Maie, M. Pruette, A. Rivera, G. Rivera and A. Sheffield for assistance during the course of the experiments and help with animal care. We also thank T. Bateman, R. Thacker and N. Travis (Clemson Bioengineering) for providing access to and assistance with mechanical testing equipment; D. Lieberman (Harvard) for providing software for measurement of limb bone cross-sectional geometry; J. Walker (University of Southern Maine) for providing access to QuickImage and QuickSAND software; and M. Ashley-Ross, A. Moran and two anonymous referees for reviewing drafts of the manuscript. Portions of this work were submitted as a Master's thesis at Clemson University by K.M.S. Support by NSF (IOB 0517340) and the Clemson University Department of Biological Sciences is gratefully acknowledged.

REFERENCES

Alexander, R. M. (1974). The mechanics of a dog jumping, *Canis familiaris*. *J. Zool. Lond.* **173**, 549-573.
Alexander, R. M. (1981). Factors of safety in the structure of animals. *Sci. Prog.* **67**, 109-130.
Alfaro, M. E., Bolnick, D. I. and Wainwright, P. C. (2005). Evolutionary consequences of many-to-one mapping of jaw morphology to mechanics in labrid fishes. *Am. Nat.* **165**, E140-E154.
Ashley, M. A., Reilly, S. M. and Lauder, G. V. (1991). Ontogenetic scaling of hindlimb muscles across metamorphosis in the tiger salamander, *Ambystoma tigrinum*. *Copeia* **1991**, 767-776.
Ashley-Ross, M. A. (1992). The comparative myology of the thigh and crus in the salamanders *Ambystoma tigrinum* and *Dicamptodon tenebrosus*. *J. Morphol.* **211**, 147-163.
Ashley-Ross, M. A. (1994a). Hindlimb kinematics during terrestrial locomotion in a salamander (*Dicamptodon tenebrosus*). *J. Exp. Biol.* **193**, 255-283.
Ashley-Ross, M. A. (1994b). Metamorphic and speed effects on hindlimb kinematics during terrestrial locomotion in the salamander *Dicamptodon tenebrosus*. *J. Exp. Biol.* **193**, 285-305.
Ashley-Ross, M. A. (1995). Patterns of hindlimb motor output during walking in the salamander *Dicamptodon tenebrosus*, with comparisons to other tetrapods. *J. Comp. Physiol.* **177**, 273-285.
Ashley-Ross, M. A. and Barker, J. U. (2002). The effect of fiber-type heterogeneity on optimized work and power output of hindlimb muscles of the salamander *Ambystoma tigrinum*. *J. Comp. Physiol. A Sens. Neural Behav. Physiol.* **188**, 611-620.
Ashley-Ross, M. A. and Bechtel, B. F. (2004). Kinematics of the transition between aquatic and terrestrial locomotion in the newt *Taricha tarosa*. *J. Exp. Biol.* **207**, 461-474.
Ashley-Ross, M. A. and Lauder, G. V. (1997). Motor patterns and kinematics during backward walking in the Pacific giant salamander: evidence for novel motor output. *J. Neurophysiol.* **78**, 3047-3060.
Beer, F. P. and Johnston, E. R., Jr (1997). *Vector Mechanics for Engineers: Statics and Dynamics*, 6th edn. Boston, MA: McGraw-Hill.
Bertram, J. E. and Biewener, A. A. (1988). Bone curvature: sacrificing strength for load predictability? *J. Theor. Biol.* **131**, 75-92.
Biewener, A. A. (1982). Bone strength in small mammals and bipedal birds: do safety factors change with body size? *J. Exp. Biol.* **98**, 289-301.
Biewener, A. A. (1983a). Locomotory stresses in the limb bones of two small mammals: the ground squirrel and chipmunk. *J. Exp. Biol.* **103**, 131-154.
Biewener, A. A. (1983b). Allometry of quadrupedal locomotion: the scaling of duty factor, bone curvature and limb orientation to body size. *J. Exp. Biol.* **105**, 147-171.
Biewener, A. A. (1989). Scaling body support in mammals: limb posture and muscle mechanics. *Science* **245**, 45-48.
Biewener, A. A. (1990). Biomechanics of mammalian terrestrial locomotion. *Science* **250**, 1097-1103.
Biewener, A. A. (1991). Musculoskeletal design in relation to body size. *J. Biomech.* **24 Suppl 1**, 19-29.
Biewener, A. A. (1992). *In vivo* measurement of bone strain and tendon force. In *Biomechanics – Structures and Systems: A Practical Approach* (ed. A. A. Biewener), pp. 123-147. New York: Oxford University Press.
Biewener, A. A. (1993). Safety factors in bone strength. *Calcif. Tissue Int.* **53 Suppl 1**, S68-S74.
Biewener, A. A. and Full, R. J. (1992). Force platform and kinematic analysis. In *Biomechanics – Structures and Systems: A Practical Approach* (ed. A. A. Biewener), pp. 45-73. New York: Oxford University Press.
Biewener, A. A. and Taylor, C. R. (1986). Bone strain: a determinant of gait and speed? *J. Exp. Biol.* **123**, 383-400.
Biewener, A. A., Thomason, J., Goodship, A. and Lanyon, L. E. (1983). Bone stress in the horse forelimb during locomotion at different gaits: a comparison of two experimental methods. *J. Biomech.* **16**, 565-576.
Biewener, A. A., Thomason, J. and Lanyon, L. E. (1988). Mechanics of locomotion and jumping in the horse (*Equus*): *in vivo* stress in the tibia and metatarsus. *J. Zool. Lond.* **214**, 547-565.
Blob, R. W. (2000). Interspecific scaling of the hindlimb skeleton in lizards, crocodilians, felids and canids: does limb bone shape correlate with limb posture? *J. Zool. Lond.* **250**, 507-531.
Blob, R. W. (2001). Evolution of hindlimb posture in non-mammalian therapsids: biomechanical tests of paleontological hypotheses. *Paleobiology* **27**, 14-38.
Blob, R. W. and Biewener, A. A. (1999). *In vivo* locomotor strain in the hindlimb bones of *Alligator mississippiensis* and *Iguana iguana*: implications for the evolution of limb bone safety factor and non-sprawling limb posture. *J. Exp. Biol.* **202**, 1023-1046.
Blob, R. W. and Biewener, A. A. (2001). Mechanics of limb bone loading during terrestrial locomotion in the green iguana (*Iguana iguana*) and American alligator (*Alligator mississippiensis*). *J. Exp. Biol.* **204**, 1099-1122.
Blob, R. W., Rai, R., Julius, M. L. and Schoenfuss, H. L. (2006). Functional diversity in extreme environments: effects of locomotor style and substrate texture on the waterfall-climbing performance of Hawaiian gobiid fishes. *J. Zool. Lond.* **268**, 315-324.
Blob, R. W., Rivera, A. R. V. and Westneat, M. W. (2008). Hindlimb function in turtle locomotion: limb movements and muscular activation across taxa, environment, and ontogeny. In *Biology of Turtles* (ed. J. Wyneken, M. H. Godfrey and V. Bels), pp. 139-162. Boca Raton, FL: CRC Press.
Butcher, M. T. and Blob, R. W. (2008). Mechanics of limb bone loading during terrestrial locomotion in river cooter turtles *(Pseudemys concinna*). *J. Exp. Biol.* **211**, 1187-1202.
Butcher, M. T., Espinoza, N. R., Cirilo, S. R. and Blob, R. W. (2008). *In vivo* strains in the femur of river cooter turtles *(Pseudemys concinna*) during terrestrial locomotion: tests of force-platform models of loading mechanics. *J. Exp. Biol.* **211**, 2397-2407.
Carrano, M. T. (1998). Locomotion in non-avian dinosaurs: integrating data from hindlimb kinematics, *in vivo* strains, and bone morphology. *Paleobiology* **24**, 450-469.
Carrier, D. R., Heglund, N. C. and Earls, K. D. (1994). Variable gearing during locomotion in the human musculoskeletal system. *Science* **265**, 651-653.
Carroll, R. L. and Holmes, R. (1980). The skull and jaw musculature as guides to the ancestry of salamanders. *Zool. J. Linn. Soc.* **68**, 1-40.
Cavagna, G. S. and Citterio, G. (1974). Effect of stretching on the elastic characteristics and the contractile component of frog striated muscle. *J. Physiol.* **239**, 1-14.
Currey, J. D. (1984). *The Mechanical Adaptations of Bones*. Princeton, NJ: Princeton University Press.
Currey, J. D. (1987). Evolution of the mechanical properties of amniote bone. *J. Biomech.* **20**, 1035-1044.
Currey, J. D. (2002). *Bones. Structures and Mechanics*. Princeton, NJ: Princeton University Press.
de Margerie, E., Sanchez, S., Cubo, J. and Castanet, J. (2005). Torsional resistance as a principal component of the structural design of long bones: comparative multivariate evidence in birds. *Anat. Rec. A Discov. Mol. Cell. Evol. Biol.* **282A**, 49-66.
Demes, B., Qin, Y., Stern, J. T., Larson, S. G. and Rubin, C. T. (2001). Patterns of strain in the macaque tibia during functional activity. *Am. J. Phys. Anthropol.* **116**, 257-265.
Diamond, J. M. (1998). Evolution of biological safety factors: a cost/benefit analysis. In *Principles of Animal Design* (ed. D. W. Weibel, C. R. Taylor and L. Bolis), pp. 21-27. Cambridge: Cambridge University Press.
Diamond, J. M. and Hammond, K. A. (1992). The matches, achieved by natural selection, between biological capacities and their natural loads. *Experientia* **48**, 551-557.
Edgren, R. A. (1960). A seasonal change in bone density in female musk turtles, *Sternothaerus odoratus* (Latreille). *Comp. Biochem. Physiol.* **1**, 213-217.
Erickson, G. M., Catanese, I. and Keaveny, T. M. (2002). Evolution of the biomechanical material properties of the femur. *Anat. Rec.* **268**, 115-124.

Flitney, F. W. and Hirst, D. G. (1978). Cross-bridge detachment and sarcomere 'give' during stretch of active frog's muscle. *J. Physiol.* **276**, 449-465.
Gao, K. and Shubin, N. H. (2001). Late Jurassic salamanders from northern China. *Nature* **410**, 574-577.
Garland, T., Jr (1998). Conceptual and methodological issues in testing the predictions of symmorphosis. In *Principles of Animal Design* (ed. D. W. Weibel, C. R. Taylor and L. Bolis), pp. 40-47. Cambridge: Cambridge University Press.
Hildebrand, M. (1975). Analysis of tetrapod gaits: general considerations and symmetrical gaits. In *Neural Control of Locomotion* (ed R. M. Herman, S. Grillner, P. S. G. Stein and D. G. Stuart), pp. 203-237. New York: Plenum Press.
Hodgskinson, R., Currey, J. D. and Evans, G. P. (1989). Hardness: and indicator of the mechanical competence of cancellous bone. *J. Orthop. Res.* **7**, 754-758.
Jayes, A. S. and Alexander, R. McN. (1980). The gaits of chelonians: walking techniques for very slow speeds. *J. Zool. Lond.* **191**, 353-378.
Kargo, W. J. and Rome, L. C. (2002). Functional morphology of proximal hindlimb muscles in the frog *Rana pipiens*. *J. Exp. Biol.* **205**, 1987-2004.
Lanyon, L. E. (1991). Biomechanical properties of bone and response of bone to mechanical stimuli: functional strain as a controlling influence on bone modeling and remodeling behavior. In *Bone, Vol. 3, Bone Matrix and Bone Specific Products* (ed. B. K. Hall), pp. 79-108. Boca Raton, FL: CRC Press.
Lieberman, D. E., Pearson, O. M., Polk, J. D., Demes, B. and Crompton, A. W. (2003). Optimization of bone growth and remodeling in response to loading in tapered mammalian limbs. *J. Exp. Biol.* **206**, 3125-3138.
Lieberman, D. E., Polk, J. D. and Demes, B. (2004). Predicting long bone loading from cross-sectional geometry. *Am. J. Phys. Anthropol.* **123**, 156-171.
Liem, K., Bemis, W., Walker, W. F. and Grande, L. (2001). Properties and mechanics of structural materials. In *Functional Anatomy of the Vertebrates: An Evolutionary Perspective*, 3rd edn. Belmont, CA: Thomson/Brooks Cole.
Lowell, R. B. (1985). Selection for increased safety factors of biological structures as environmental unpredictability increases. *Science* **228**, 1009-1011.
Lutz, G. J. and Rome, L. C. (1994). Built for jumping: the design of the frog muscular system. *Science* **263**, 370-372.
Lutz, G. J. and Rome, L. C. (1996). Muscle function during jumping in frogs. II. Mechanical properties of muscle: implications for system design. *Am. J. Physiol.* **271**, C571-C578.
Main, R. P. and Biewener, A. A. (2004). Ontogenetic patterns of limb loading, *in vivo* bone strains and growth in the goat radius. *J. Exp. Biol.* **207**, 2577-2588.
Main, R. P. and Biewener, A. A. (2007). Skeletal strain patterns and growth in the emu hindlimb during ontogeny. *J. Exp. Biol.* **210**, 2676-2690.
Peplowski, M. M. and Marsh, R. L. (1997). Work and power output in the hindlimb muscles of Cuban tree frogs *Osteopilus septentrionalis* during jumping. *J. Exp. Biol.* **200**, 2861-2870.
Petranka, J. W. (1998). *Salamanders of the United States and Canada*. Washington, DC: Smithsonian Institution Press.
Reilly, S. M., Willey, J. S., Biknevicius, A. R. and Blob, R. W. (2005). Hindlimb function in the alligator: integrating movements, motor patterns, ground reaction forces and bone strain of terrestrial locomotion. *J. Exp. Biol.* **208**, 993-1009.
Reilly, S. M., McElroy, E. J., Odum, R. A. and Hornyak, V. A. (2006). Tuataras and salamanders show that walking and running mechanics are ancient features of tetrapod locomotion. *Proc. R. Soc. B* **273**, 1563-1568.
Roberts, T. J. and Marsh, R. L. (2003). Probing the limits to muscle-powered accelerations: lessons from jumping bullfrogs. *J. Exp. Biol.* **206**, 2567-2580.
Ross, C. F. and Metzger, K. A. (2004). Bone strain gradients and optimization in vertebrate skulls. *Ann. Anat.* **186**, 387-396.
Rubin, C. T. and Lanyon, L. E. (1982). Limb mechanics as a function of speed and gait: a study of functional strains in the radius and tibia of horse and dog. *J. Exp. Biol.* **101**, 187-211.
Suzuki, H. K. (1963). Studies on the osseous system of the slider turtle. *Ann. N. Y. Acad. Sci.* **109**, 351-410.
Wainwright, P. C., Alfaro, M. E., Bolnick, D. I. and Hulsey, C. D. (2005). Many-to-one mapping of form to function: a general principle in organismal design? *Int. Comp. Biol.* **45**, 256-262.
Wainwright, S. A., Biggs, W. D., Currey, J. D. and Gosline, J. M. (1976). *Mechanical Design in Organisms*. Princeton, NJ: Princeton University Press.
Walker, J. A. (1998). Estimating velocities and accelerations of animal locomotion: a simulation experiment comparing numerical differentiation algorithms. *J. Exp. Biol.* **201**, 981-995.
Walker, W. F., Jr (1973). The locomotor apparatus of Testudines. In *Biology of the Reptilia, Vol. 4, Morphology D* (ed. C. Gans and T. S. Parsons), pp. 1-100. London: Academic Press.
Wilson, M. P., Espinoza, N. R., Shah, S. R. and Blob, R. W. (2009). Mechanical properties of the hindlimb bones of bullfrogs and cane toads in bending and torsion. *Anat. Rec.* **292**, 935-944.
Wink, C. S. and Elsey, R. M. (1986). Changes in femoral morphology during egg-laying in *Alligator mississippiensis*. *J. Morphol.* **189**, 183-188.